Large-eddy simulations of fluid-structure interaction problems

Jianming Yang, Sergio Preidikman and Elias Balaras*

Department of Mechanical Engineering,

University of Maryland,

College Park, MD 20742, USA

Abstract

In the present paper we present a methodology that is applicable to large-eddy simulations of fluid structure interaction problems. The fluid flow equations are solved on a fixed grid that does not conform to the structure, and boundary conditions are imposed using a local reconstruction procedure. The structure that undergoes both linear-elastic and large-angle/large-displacement rigid body motions is strongly coupled to the fluid using a predictor-corrector approach. Preliminary results for both laminar and turbulent flow problems are included.

Keywords: fluid/structure interaction, large-eddy simulation, sharp interface method, immersed boundary method.

*Contact e-mail: balaras@eng.umd.edu.

1 Introduction

Numerical simulations of turbulent and transitional flows with dynamically moving boundaries are amongst the most challenging problems in computational mechanics. Although a variety of fluid-structure interaction algorithms has been developed over the years, relatively few applications in turbulent and transitional flows have been reported. In most cases, this is due to prohibitively high computational cost, or dissipative discretizations that limit the applicability of such methods to classical turbulence modeling strategies. Further advancements in this field can be achieved by coupling state-of-the-art tools to model turbulence and transition (i.e. large-eddy simulations (LES) or hybrid formulations) with cost/efficient numerical methods applicable to problems with large boundary motions and deformations. Example applications of such a tool include a variety of low and moderate Reynolds number turbulent flow problems from engineering, biology, and medicine, where fluid/structure interactions are central to the dynamics of the flow.

In the present paper we present a non-boundary conforming method that is applicable to LES of fluid-structure interaction problems. In such case the grid does not need to conform to a complex moving body, eliminating the tedious grid regeneration or deformation procedure required in classical boundary-conforming approaches, and at the same time allowing the adoption of highly efficient, energy conserving, Cartesian solvers. The boundary motion which is strongly coupled to the fluid flow, can be due to linear-elastic and large-angle/large displacement rigid-body motions. The overall

methodology including the fluid solver, the structural model and their coupling will be discussed briefly in the next section. Then some preliminary results on simple two-dimensional configurations and fully three-dimensional turbulent flows will be given to demonstrate the accuracy and range of applicability of the method, respectively.

2 Methodology

In LES, the resolved, large-scale, velocity, and pressure fields can be obtained by directly solving the filtered Navier-Stokes equations, where scales smaller than the grid size will be modeled. In the present implementation a top-hat filter in physical space is implicitly applied by the finite-difference operators. The resulting subgrid scale (SGS) stresses are modeled using the Lagrangian, dynamic, eddy-viscosity model [2]. The equations governing the evolution of the large scales are solved on a fixed Cartesian grid that covers the entire computational domain, ignoring the presence of complex immersed bodies. A fractional-step method is used for this purpose, where all terms are advanced in time using an explicit third-order Runge-Kutta scheme. All spatial derivatives are approximated with second order central differences on a staggered grid.

Boundary conditions on a complex immersed structure, which in general is not aligned with the grid, are enforced using a 'direct-forcing' scheme that practically reconstructs the solution in the vicinity of the body according to the target boundary values. An example of an immersed boundary identified by a series of material-fixed interfacial markers whose location is defined in the reference configuration of the solid, is shown in Fig. 1. This information is used to identify the Eulerian grid nodes that are involved in

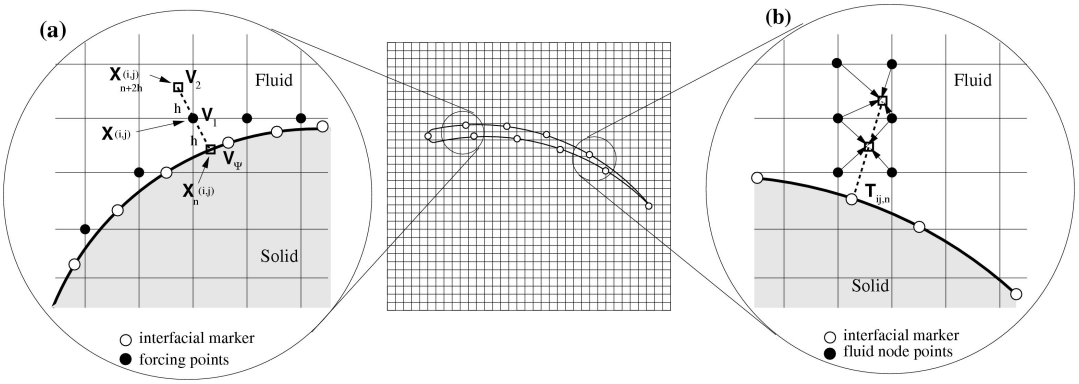

Figure 1: Schematic of a solid body immersed in a Cartesian grid. (a) Reconstruction of the velocity field near the interface; (b) Reconstruction of the traction forces on the body. Dashed line denotes the normal the boundary.

the solution reconstruction, which is performed "around" the points in the fluid phase closest to the solid boundary (see Fig 1a). An advantage of this choice is that it simplifies the treatment for the points that emerge from the solid as the boundary moves through the fixed grid. Details on the overall methodology can be found in [1].

In the reconstruction procedure described above it was assumed that the local boundary velocity is known. This velocity, however, has to be computed from the solid structure that can undergo both linear-elastic and large-angle/large-displacement rigid body motions. In order to describe the dynamics of the body, the state of the structure and the loads time-change are tracked. This tracking process necessarily involves a kinematic description with respect to a reference state. In the present study the corotational (CR) formulation is used [3]. A linear finite-element model of the structure is used to predict the elastic deformations. The models are coupled in such a way that the structural and hydrodynamic grids can be chosen arbitrarily. The deformation of the structure is expressed as an expansion in terms of the linear free-vibration modes obtained from the

finite-element model. The time-dependent coefficients in the expansion of the deflection are the generalized coordinates of the complete dynamic system.

A strong coupling scheme is adopted, where the fluid and the structure are treated as elements of a single dynamical system, and all of the governing equations are integrated simultaneously, and interactively in the time-domain. There is a fundamental complication related to the time-domain approach: to predict the hydrodynamic loads one must know the motion of the structure, and to predict the motion of the structure one must know the hydrodynamic loads. To overcome this complication, an iterative scheme that accounts for the interaction between the hydrodynamic loads and the motion of the structure was developed. The procedure is based on Hamming's, fourth-order, predictor-corrector method. Details can be found in [4, 5].

3 Results

3.1 Vortex-induced vibrations for a circular cylinder

As a demonstration of the accuracy and robustness of the proposed method, vortex-induced vibrations (VIV) for a circular cylinder are simulated. The equation of motion for VIV of a circular cylinder oscillating in X and Y directions modeled by a spring-damper-mass system is:

$$[m]\ddot{\mathbf{x}}(t) + [c]\dot{\mathbf{x}}(t) + [k]\mathbf{x}(t) = \mathbf{F}(\mathbf{x}, \dot{\mathbf{x}}, \ddot{\mathbf{x}}; t), \tag{1}$$

where $[m]$ is the mass matrix, $[c]$ is the damping matrix, and $[k]$ is the stiffness matrix for the structure. $\mathbf{F}$ is the fluid force, and $\mathbf{x}(t) = X_0(t)\mathbf{i} + Y_0(t)\mathbf{j}$, with $X_0(t)$ and $Y_0(t)$ the displacements of the center of mass of the cylinder in the x and y directions, respectively.

Two different cases were considered with one- and two-degrees-of-freedom respectively. The Reynolds number, $Re = U_\infty D/\nu = 200$ (U_∞ the freestream velocity, D the diameter of the cylinder, and ν the kinematic viscosity of the fluid) for both cases. The computational domain is a rectangular box, and the cylinder center was initially located at $(0, 0)$. A Cartesian grid of 640×480 grid points in x and y directions is used with approximately uniform cells of size $0.01D^2$ in the vicinity of the cylinder.

For the flow in the first case (the cylinder is allowed to vibrate in the transverse direction), the Skop-Griffin parameter $S_G = 2\pi^3 S^2(m^*\zeta) = 7.460 \times 10^{-3}$ (S the Strouhal number of the fixed cylinder, m^* the mass ratio, and ζ the damping ratio). Our results are in very good agreement with results in the literature. Using for example the empirical equation by Sarpkaya [7], $A^*_{MAX} = B/(C + S_G^2)^{0.5}$, (where $B = 0.385$ and $C = 0.120$), one can obtain $A^*_{MAX} = 1.111$ for the above parametric space, while our simulation predicts $A^*_{MAX} = 1.118$, which is in good agreement.

More detailed results are shown for the problem with two-degrees-of-freedom (the cylinder can respond to both the transverse and streamwise forces). Fig.2(a) shows the vortex pattern: the vortices shed from the cylinder develop into two parallel rows of vortices with opposite sign. We observe similar vortex shedding pattern for the one degree-of-freedom case above, but this is very different from the Karman vortex street in the wake of fixed circular cylinder, which presents vortices with alternate signs in one

row behind the cylinder. In Fig.2(b) the time histories of drag and lift coefficients are shown. Since the simulation is started from the steady solution of the fixed cylinder case, the flow field develops into steady state with almost constant amplitudes of C_D and C_L rapidly after a short transition period. Fig.2(c) shows the $X - Y$ phase plot, where the red line identifies the steady state. A symmetric trajectory is obtained at the steady state. Here the peak amplitude is $A^*_{MAX} = 1.294$, which is larger than that of the one-degree-of-freedom case.

3.2 Turbulent flow over a traveling wavy wall

In this section LES of turbulent flow over a flexible wavy wall undergoing transverse motion in a form of streamwise traveling wave is presented. The immersed boundary in this case no longer belongs to a moving rigid body, but it has a non-uniform prescribed velocity varying with time. Nevertheless, given the availability of accurate DNS data in the literature [6], we can use it to test the accuracy and efficiency of the proposed algorithm in turbulent flows. The parametric space and computational box in these LES are the same as in the reference DNS by Shen *et al.* [6], where the location of the wall boundary as a function of time is given by, $y_w(t) = a \sin k(x - ct)$ (a is the magnitude of the oscillation, $k = 2\pi/\lambda$ is the wavenumber, λ is the wavelength, and c is the phase speed of the traveling wave).

A grid of $288 \times 88 \times 64$ (streamwise, vertical, and spanwise direction, respectively) is used here for all the simulations. The grid is uniform in the streamwise and spanwise homogeneous directions, and is stretched in the vertical direction. In Fig. 3 the

instantaneous vortical structures visualized using isosurfaces of the second invariant of the velocity gradient tensor, Q, are shown for $c/U = 0.0$ and $c/U = 0.4$ (c/U is the ratio of the wave speed to the freestream velocity). It can be seen that the strong streamwise vortices that are characteristic of stationary wavy walls ($c/U = 0$) are suppressed as c/U increased from 0.0 to 0.4. Similar behavior has been observed in the reference DNS [6]. Quantitative comparisons are shown in Fig. 4, where the variations of F_f and F_p as functions of the phase speed of the traveling wavy wall, c/U, are shown (F_f is the total friction force, F_P is total pressure force on the wall in the streamwise direction, respectively). Here again our data are in good agreement with the reference simulation [6].

References

[1] Balaras, E. 2004. Modeling complex boundaries using an external force field on fixed Cartesian grids in large-eddy simulations. *Computers & Fluids*, **33**, 375–404.

[2] Meneveau, C., Lund, T.S., and Cabot, W. H. 1996. A Lagrangian dynamic subgrid-scale model of turbulence. *J. Fluid Mech.* **319**, 353–.

[3] A. H. Nayfeh, S. Emam, S. Preidikman, and D. T. Mook, 2003. An Exact Solution for the Natural Frequencies of Flexible Beams Undergoing Overall Motion. *Journal of Vibration and Control*, **9**, 1221–1229.

[4] S. Preidikman and D. T. Mook, 1997. Numerical simulation of flutter of suspension bridges. *Applied Mechanics Reviews*, **50**, 174–179.

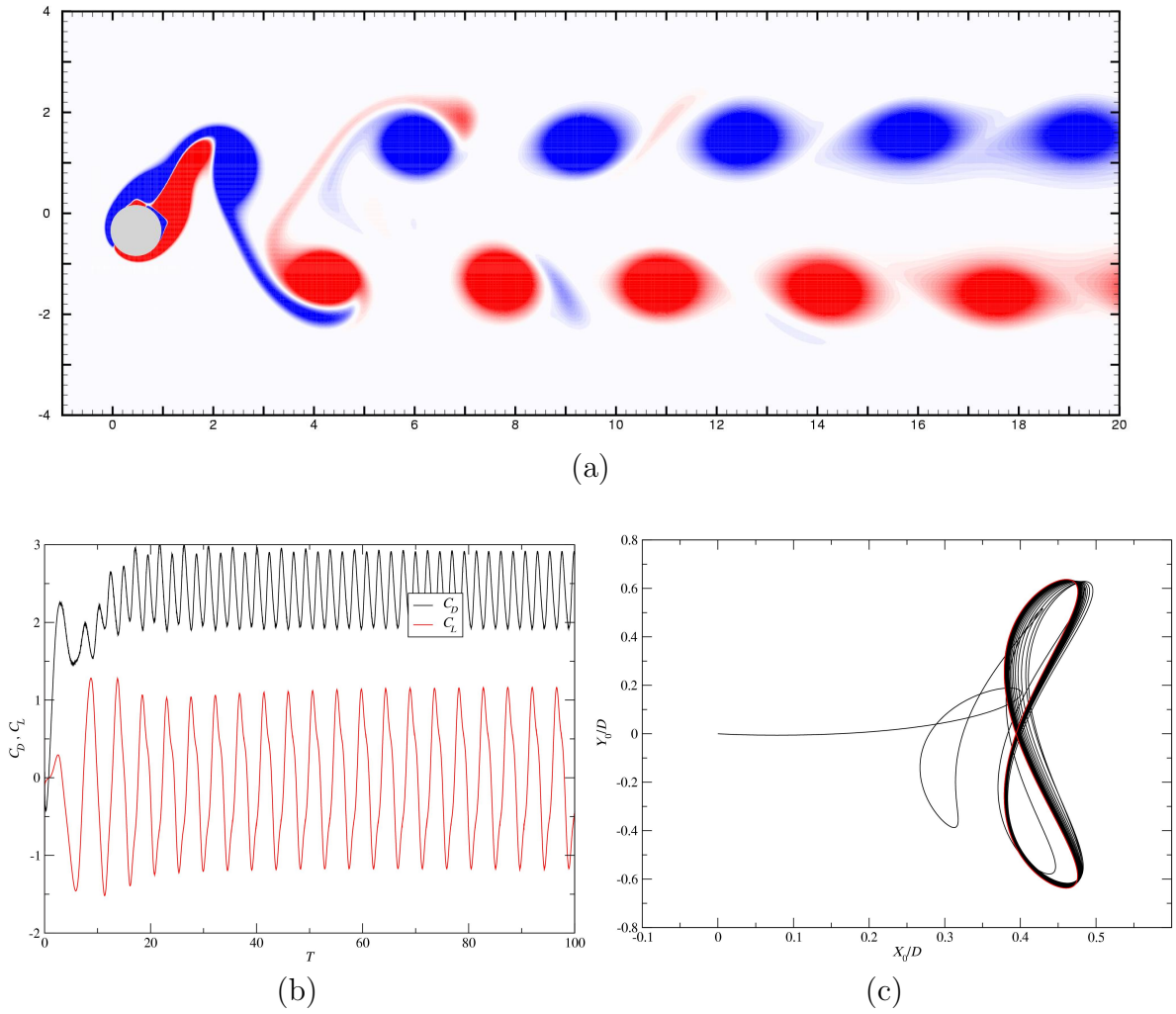

Figure 2: Vortex-induced vibrations of an elastic circular cylinder: (a) Vortex pattern; (b) Force coefficients and displacement versus time; (c) $X - Y$ phase plot.

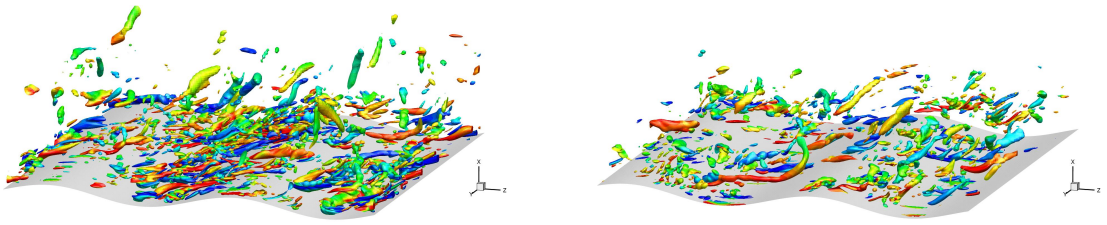

(a) (b)

Figure 3: Turbulent flow over a traveling wavy wall. Instantaneous vortical structures colored by streamwise vorticity. (a) $c/U = 0.0$ and (b) $c/U = 0.4$.

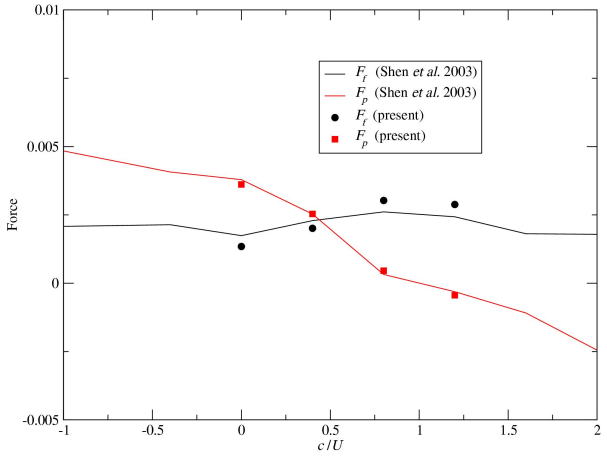

Figure 4: Variation of the force acting on the traveling wavy wall.

[5] S. Preidikman and D. T. Mook, 2000. Time-Domain Simulations of Linear and Non-Linear Aeroelastic Behavior. *Journal of Vibration and Control*, **6**, 1135–1176.

[6] Shen, L. *et al.*, 2003. Turbulent flow over a flexible wall undergoing a streamwise traveling wave motion. *J. Fluid Mech.* **484**, 197–221.

[7] Williamson, C.H.K., Govardhan, R., 2004. Vortex-induced vibrations. *Annu. Rev. Fluid Mech.* **36**: 413-455.